Circuit QED with a quantum-dot charge qubit dressed by Cooper pairs

L. E Bruhat,[1,2] T. Cubaynes,[1] J. J. Viennot,[3] M. C. Dartiailh,[1] M. M. Desjardins,[1] A. Cottet,[1] and T. Kontos[1,*]

[1]*Laboratoire Pierre Aigrain, Ecole Normale Supérieure-PSL Research University, CNRS, Université Pierre et Marie Curie-Sorbonne Universités, Université Paris Diderot-Sorbonne Paris Cité, 24 rue Lhomond, F-75231 Paris Cedex 05, France*

[2]*Microtechnology and Nanoscience, Chalmers University of Technology, Kemivägen 9, SE-41296 Gothenburg, Sweden*

[3]*JILA and the Department of Physics, University of Colorado, Boulder, Colorado 80309, USA*

(Received 10 July 2018; revised manuscript received 28 September 2018; published 18 October 2018)

Coupling double-quantum-dot circuits to microwave cavities provides a powerful means to control, couple, and manipulate qubits based on the charge or spin of individual electrons. Here, we revisit this standard configuration by adding superconductivity to the circuit. We combine theory and experiment to study a superconductor–double-quantum-dot circuit coupled to microwave cavity photons. First, we use the cavity as a spectroscopic probe. This allows us to determine the low-energy spectrum of the device and to reveal directly Cooper-pair-assisted tunneling between the two dots. Second, we observe a vacuum Rabi splitting which is a signature of strong charge photon coupling and a premiere with carbon-nanotube-based quantum-dot circuits. We show that our circuit design intrinsically combines a set of key features to achieve the strong coupling regime to the cavity. A low charging energy reduces the device sensitivity to charge noise, while sufficient coupling is provided by the shaping of the spectrum of the double quantum dot by the superconducting reservoir. Our findings could be adapted to many other circuit designs and shed light on the coupling of superconducting nanoscale devices to microwave fields.

DOI: 10.1103/PhysRevB.98.155313

I. INTRODUCTION

Circuit quantum electrodynamics (cQED) allows one to probe, manipulate, and couple superconducting quantum bits at an exquisite level using cavity photons. Transferring the methods of cavity quantum electrodynamics to quantum dots circuits is appealing for multiple reasons [1]. Electrons confined in quantum dots can be used as quantum bits based on their spin or charge degree of freedom. In the context of quantum information processing, cavity photons were first envisioned as a powerful way to manipulate such quantum bits. Therefore, most experimental efforts [2–8] have been directed towards achieving the strong coupling regime, which allows one to hybridize coherently light and matter [9]. To that purpose, tunneling between the double quantum dot and metallic contacts is usually considered as an undesired dissipation channel and minimized.

However, metallic reservoirs can also be seen as a resource, as quantum-dot circuits can include a variety of normal metal, ferromagnetic, or superconducting electrodes. The engineering of electronic states in devices combining materials with different electronic properties is at the heart of many recent methods put forward for quantum information processing. One particularly promising venue is the coupling of superconductors to nanoconductors. For example, semiconducting nanowires proximitized by superconductors are under active investigation because of the possibility to induce nonlocal superconducting correlations in the topological regime [10,11]. Double quantum dots with a central superconducting contact are sought for creating distant entangled spins by the splitting of Cooper pairs [12–15].

Combining cQED architectures with hybrid superconducting mesoscopic circuits is only at its premises. This has been successful in the case of superconducting quantum point contacts, as epitomized by the recent manipulation of an Andreev qubit by a microwave resonator [16]. Looking at hybrid superconductor quantum-dot circuits, a single experiment has been reported so far, with a single dot [17].

Here, we present the first implementation of a hybrid superconductor–double-quantum-dot circuit coupled to a microwave cavity. Such an experiment was theoretically proposed to test the coherence of Cooper pair splitting between the two dots [18,19]. As we will show below, our circuit operates in a parameter regime where the coherent injection of Cooper pair appears in a different way as was theoretically considered in those references. Nevertheless, our results confirm the idea that cQED tools are a powerful method to probe the spectrum of hybrid superconductor–quantum-dot circuits. Surprisingly, our work also demonstrates the reciprocal, namely, that adding a superconducting electrode to a double-quantum-dot circuit can be instrumental in building a strongly coupled mesoscopic cQED system.

As observed in previous experiments, the cavity transmission shows a resonance between the cavity mode and a circuit transition. We find that the behavior of our hybrid double dot is dominated by tunnel coupling between the left and the right dot, which results in a "charge-qubit"-like transition. However, the cavity transmission reveals the shaping of the spectrum of the double quantum dot by the superconducting reservoir. This represents the first spectroscopic observation of Cooper-pair-assisted cotunneling between the left and the

*Corresponding author.

right dots [20–22], in equilibrium conditions. So far, this effect had been observed only indirectly through out-of-equilibrium transport measurements [23,24]. We present a theoretical description of the eigenenergies and eigenmodes of the dressed superconductor–charge qubit. The interplay between bare interdot tunneling and the superconducting proximity effect was not considered in previous derivations of the spectrum of superconductor–double quantum dots. Our theoretical results are validated by their ability to reproduce the very peculiar features of our measurements.

Importantly, the superconductor does not only modify the spectrum but also the electron-photon coupling. In addition to the usual coupling mechanism where cavity photons modulate the energy difference between the two dots, our theoretical model clearly highlights the possibility of coupling via a symmetric modulation of the dot energies. In presence of a superconducting central electrode, such a common-mode excitation effectively results in a strong sensitivity of the double-dot tunnel barrier to the cavity electric field. This corresponds to the original driving mechanism proposed by DiVincenzo [25–28], which is implemented here in a cavity.

Our coupling mechanism is more than a simple curiosity as it actually provides a way to reach the strong coupling regime between the cavity and our modified charge qubit. Such a regime was obtained recently using two different approaches [7,8]. Mi *et al.* built their double quantum dot in a low charge noise material, namely, SiGe. Stockklauser *et al.* used a squid array resonator to boost the value of the electron-photon coupling. Here, we demonstrate a third approach: the common-mode coupling scheme allows us to decrease the charging energy of our device and correspondingly decrease the device sensitivity to charge noise, while keeping a sufficient coupling strength. It is worth noting that the strong electron-photon coupling was also obtained with the spin degree of freedom very recently [29–31].

This paper is organized as follows. Section II presents our experimental setup. Section III presents our theoretical derivation of the spectrum of the hybrid superconductor–charge qubit in absence of the cavity. Section IV gives and discusses the expression of the coupling of the dressed charge qubit to the cavity. The theoretical description is confronted to experimental data in Sec. V. Section VI shows our experimental observation of the strong coupling regime. Section VII summarizes our results and gives various perspectives. Appendices A, B, and C provide experimental, theoretical, and simulation details, respectively.

II. SAMPLE AND MEASUREMENT SETUP

We use carbon-nanotube-based double-quantum-dot circuits embedded in a high-finesse superconducting microwave cavity [6,32,33]. The microwave cavity is a Nb coplanar waveguide cavity with resonance frequency of about 6.636 GHz and a quality factor of about 16 000. Throughout the paper, we describe results obtained with two different devices (samples A and B) which had exactly the same layout. Figures 1(a)–1(c) show optical as well as scanning electron microscope pictures of one of our devices. A single-wall carbon nanotube is tunnel coupled to a central superconducting finger (in orange) and two outer nonsuperconducting electrodes (in blue). Two side gates (in green) are used to tune the double-dot energy levels. A finger galvanically coupled to the central conductor of our cavity (in red) is attached to two top gates in a fork geometry. This coupling scheme is markedly different from the double-dot/cavity coupling schemes used so far in that context [2,3,5–8]. Instead of favoring a microwave modulation of the difference of the energy between the left and the right dots, the fork geometry shown in Fig. 1(c) favors the modulation of the sum of the left and right dot energies by microwave photons.

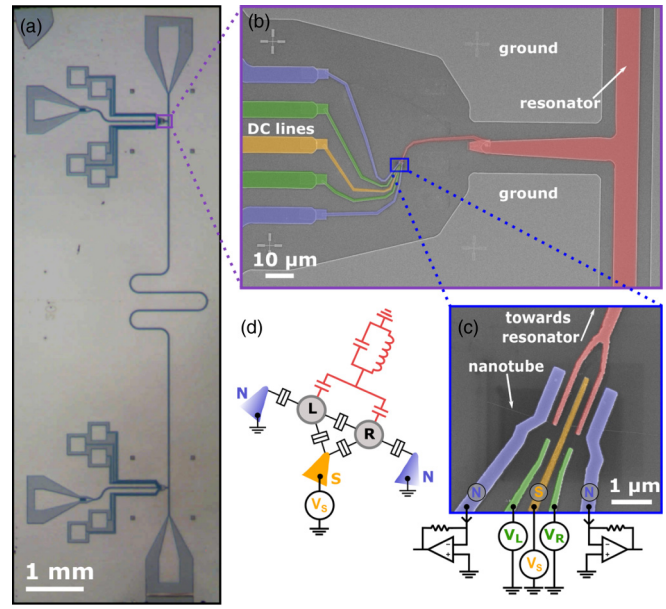

FIG. 1. (a) Optical photograph of the layout of our cavity QED architecture on a large scale. (b), (c) SEM micrographs of our devices on two different scales in false colors. The "fork" coupling gate is colored in red. The superconducting electrode is colored in orange. The normal (nonsuperconducting) electrodes are colored blue. The gates are colored in green. (d) Circuit diagram of our hybrid double quantum dot highlighting the symmetric coupling scheme between the two dots and the resonator in red.

All the measurements have been carried out at about 18 mK. We simultaneously measure dc transport through the quantum-dot device and microwave transmission through the coplanar waveguide resonator. Our control parameters of the quantum-dot circuit are the bias voltage V_S applied to the superconducting electrode and the gate voltages V_L and V_R. For convenience, measurements are often taken in the rotated frame V_Σ-V_δ, as defined in Appendix A. Concerning the cavity, the tunable parameters are the frequency and power of the probe tone. Details about sample fabrication and measurement setup are given in Appendix A.

From the transport measurement shown in Fig. 2(a) we are able to assess the electrical contact between the double dot and a superconducting reservoir. We measure a superconducting gap Δ of about 150 μeV. The fact that we do not observe any measurable subgap currents indicate that our tunnel barriers are rather opaque. In the following, transport data will be omitted, as it would be blank at most working points (see Appendix A). However, we will show that cavity signals can be very strong and contain signatures of tunneling processes

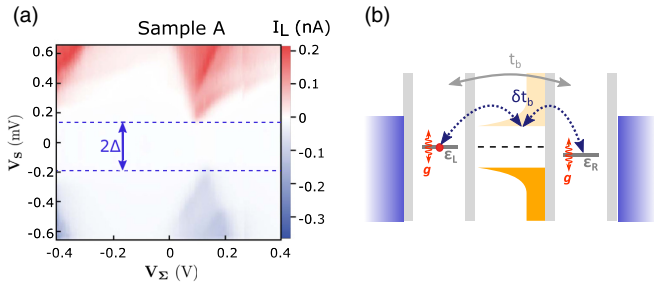

FIG. 2. (a) Color scale map of the current I_L flowing through the left (L) normal metal contact as a function of bias voltage V_S and the gate voltage V_Σ for sample A. From this map, we read off a superconducting gap $\Delta \sim 150\ \mu$eV. (b) Cotunneling scheme accounting for the renormalization of the hopping constant between the left and the right quantum dots.

between the dots and the superconducting lead. This is mainly because the charge-qubit transition of a double dot is modified by the superconducting reservoir, as we explain now.

III. LOW-ENERGY SPECTRUM OF THE HYBRID SUPERCONDUCTOR DOUBLE DOT IN THE ABSENCE OF THE CAVITY

Contrarily to normal contacts, a superconducting contact is expected to modify coherently the spectrum of a double quantum dot. Let us first recall the double-dot spectrum in absence of superconductor. The double-dot Hamiltonian reads as $H_{\rm DQD} = \epsilon_L\ \hat{n}_L + \epsilon_R\ \hat{n}_R + t_b(c^\dagger_{L\uparrow}c_{R\uparrow} + c^\dagger_{L\downarrow}c_{R\downarrow}) + \text{H.c.} + U_m\hat{n}_L\hat{n}_R + \frac{1}{2}U_L\hat{n}_L(\hat{n}_L - 1) + \frac{1}{2}U_R\hat{n}_R(\hat{n}_R - 1)$ where, for each dot $i \in \{L, R\}$, ϵ_i denotes the orbital energy, U_i the charging energy, $c^\dagger_{i\sigma}$ the electron creation operator with spin $\sigma \in \{\downarrow, \uparrow\}$, and $\hat{n}_i$ the electron number operator. The mutual charging energy between the two dots is U_m and t_b is the direct hopping strength between the L and the R dots. Close to the (0,1)/(1,0) degeneracy line, the relevant eigenstates are the antibonding and bonding states: $|+\rangle = u|L\rangle + v|R\rangle$, $|-\rangle = -v|L\rangle + u|R\rangle$ with the eigenenergies $E_\pm = \frac{-U_m + \epsilon_\Sigma \pm \sqrt{\epsilon_\delta^2 + 4t_b^2}}{2}$, where $\epsilon_\delta = \epsilon_L - \epsilon_R$, $u = \sqrt{\frac{1}{2} - \frac{1}{2}\frac{\epsilon_\delta}{\sqrt{\epsilon_\delta^2+4t_b^2}}}$, and $v = \sqrt{\frac{1}{2} + \frac{1}{2}\frac{\epsilon_\delta}{\sqrt{\epsilon_\delta^2+4t_b^2}}}$. This gives a transition energy of the double quantum dot: $\hbar\omega_{\rm DQD} = E_+ - E_- = \sqrt{\epsilon_\delta^2 + 4t_b^2}$. We will see below that this quantity is deeply modified by the presence of the superconducting lead.

Figure 2(b) gives a qualitative picture of the main process responsible for dressing the bonding and antibonding states of a double-dot charge qubit. In addition to the bare tunneling between the two dots (gray solid arrow), the superconductor induces cotunneling processes: an electron from one dot can virtually excite a quasiparticle in the superconductor and tunnel to the other dot (blue dotted arrows).

We now outline the formal derivation of the spectrum of the double quantum dot in presence of a superconductor (see Appendix B for details). We start by considering the Hamiltonian of our double-quantum-dot–superconductor device $H = H_{\rm DQD} + H_S + H_{S-\rm DQD}$, which naturally contains the double-quantum-dot Hamiltonian $H_{\rm DQD}$ discussed above. Additionally, there is a term describing the quasiparticles in the superconductor: $H_S = \sum_{k\sigma} E_k \gamma^\dagger_{k\sigma}\gamma_{k\sigma}$ where $\gamma^\dagger_{k\sigma}$ ($\gamma_{k\sigma}$) are the creation (annihilation) Bogoliubov quasiparticle operators. Finally, $H_{S-\rm DQD}$ accounts for electron tunneling between the superconductor and the two dots and can be written $H_{S-\rm DQD} = \sum_{k\sigma, i\in\{L,R\}} t_i^* \mathcal{A}^i_{k\sigma} c^\dagger_{j\sigma} + \text{H.c.}$ where $t_i \equiv \sqrt{\Gamma_{Si}}$ is the hopping strength between the superconductor and dot i and $\mathcal{A}^i_{k\sigma}$ is a linear combination of Bogoliubov operators (formula given in Appendix B). At second order in t_i, the states $|+\rangle$ and $|-\rangle$ become coupled to the singlet and triplet states: $|S\rangle, |T_0\rangle, |T_+\rangle, |T_-\rangle$, whose energies are, close to the degeneracy line, $E_S = E_{T_0} = E_{T_+} = E_{T_-} \simeq \epsilon_L + \epsilon_R + U_m \equiv \epsilon_\Sigma$.

The low-energy spectrum of the system can be obtained by a Schrieffer-Wolf transformation $\hat{H} = e^{-S}\hat{H}e^S$ corresponding to "tracing out" the superconducting quasiparticles. Taking the same path as previous theoretical work on Cooper pair splitters [34,35], we look for the appropriate S operator which eliminates $H_{S-\rm DQD}$ to first order, resulting in an effective Hamiltonian to second order in the tunnel couplings t_i of the superconductor to the two dots. While this method is well known, it had so far always been applied to the case of two completely decoupled dots, namely, $t_b = 0$. By including a finite hopping t_b between the left and the right dots, our derivation yields results which are crucial to interpret our experimental findings.

Projecting the effective Hamiltonian on the subspace $\{|+\rangle, |-\rangle\}$, we get $\hat{H}_{\rm eff} = (E_+ + \delta E_+)|+\rangle\langle+| + (E_- + \delta E_-)|-\rangle\langle-| + \delta t_b|+\rangle\langle-| + \delta t_b|-\rangle\langle+|$.

Below, we focus close to the degeneracy line between (0,1)/(1,0) charge states but the (1,1)/(0,2) lines give rise to similar expressions. After tedious but straightforward calculations, the perturbative elements have the following expressions:

$$\delta t_b = (\Gamma_{SR} - \Gamma_{SL})\frac{t_b}{\sqrt{\epsilon_\delta^2 + 4t_b^2}}\left\{4Ln\frac{2\hbar\omega_D}{\Delta} + \pi\frac{U_m}{\Delta} + \frac{{U_m}^2 + {\epsilon_\Sigma}^2 + {\epsilon_\delta}^2 + 4{t_b}^2}{\Delta^2}\right\} - \pi t^0_{eh}\frac{\epsilon_\Sigma}{\Delta}\frac{\epsilon_\delta}{\sqrt{\epsilon_\delta^2 + 4t_b^2}}\left(1 - \frac{2}{\pi}\frac{U_m}{\Delta}\right), \quad (1)$$

$$\delta E_+ = (\Gamma_{SR} - \Gamma_{SL})\frac{\epsilon_\delta}{\sqrt{\epsilon_\delta^2 + 4t_b^2}}\left\{Ln\frac{2\hbar\omega_D}{\Delta} - \frac{\pi}{2}\frac{U_-}{\Delta} + \frac{U_-^2 + {\epsilon_\Sigma}^2}{\Delta^2}\right\}$$

$$- \frac{\pi}{2}\frac{\epsilon_\Sigma}{\Delta}(\Gamma_{SR} + \Gamma_{SL})\left(1 - \frac{1}{\pi}\frac{U_-}{\Delta}\right) + \pi t^0_{eh}\frac{\epsilon_\Sigma}{\Delta}\frac{t_b}{\sqrt{\epsilon_\delta^2 + 4t_b^2}}\left(1 - \sqrt{\frac{2|\delta r|}{\pi\xi_0}}\frac{U_-}{\Delta}\right), \quad (2)$$

$$\delta E_- = -(\Gamma_{SR}-\Gamma_{SL})\frac{\epsilon_\delta}{\sqrt{\epsilon_\delta^2+4t_b^2}}\left\{Ln\frac{2\hbar\omega_D}{\Delta}-\frac{\pi}{2}\frac{U_+}{\Delta}+\frac{U_+^2+{\epsilon_\Sigma}^2}{\Delta^2}\right\}$$
$$-\frac{\pi}{2}\frac{\epsilon_\Sigma}{\Delta}(\Gamma_{SR}+\Gamma_{SL})\left(1+\frac{1}{\pi}\frac{U_+}{\Delta}\right)-\pi t_{eh}^0\frac{\epsilon_\Sigma}{\Delta}\frac{t_b}{\sqrt{\epsilon_\delta^2+4t_b^2}}\left(1+\sqrt{\frac{2|\delta r|}{\pi\xi_0}}\frac{U_+}{\Delta}\right), \quad (3)$$

where t_{eh}^0 is the Cooper pair splitting amplitude [see Eq. (B8) in Appendix B], δr is the distance between tunnel contacts from the superconductor to each dot, ξ_0 is the superconducting coherence length, and ω_D is the Debye frequency, used as a cutoff. The following notation was introduced: $U_\pm = \pm U_m + \sqrt{\epsilon_\delta^2+4t_b^2}$. The eigenenergies are $\tilde{E}_\pm = \frac{E_+ + \delta E_+ + E_- + \delta E_- \pm \sqrt{(E_+ + \delta E_+ - E_- - \delta E_-)^2 + \delta t_b^2}}{2}$ which leads to a transition energy of the form $\hbar\omega_{S-\mathrm{DQD}} = \sqrt{(\epsilon_\delta^2+4t_b^2)Z(\epsilon_\delta,\epsilon_\Sigma)^2 + t(\epsilon_\delta,\epsilon_\Sigma)^2}$, with $Z(\epsilon_\delta,\epsilon_\Sigma) = 1+\frac{\delta E_+ - \delta E_-}{E_+ - E_-}$ and $t(\epsilon_\delta,\epsilon_\Sigma) = \delta t_b$. It is important to notice here the major modification induced by the superconductor: the transition energy of the circuit does now also depend on the sum of the two dot energies ϵ_Σ, rather than only on their difference ϵ_δ.

Before concluding this section, we would like to point out that the calculation is essentially the same if there is an additional quantum number (e.g., a valley quantum number) ruling the states of the double quantum dot. This naturally leads to a second transition similar to the one considered above but with different parameters. This can account for the two-transition structure which is used to understand quantitatively our experimental findings.

IV. ELECTRON-PHOTON COUPLING OF THE HYBRID DOUBLE QUANTUM DOT

We now evaluate the effect of the superconductor on the coupling to the cavity. The conventional coupling mechanism of a double quantum dot to the cavity in the absence of the superconductor takes the form

$$\langle +|\,(g_L\,\hat{n}_L + g_R\,\hat{n}_R)\,(\hat{a}+\hat{a}^\dagger)\,|-\rangle = uv(g_L-g_R)(\hat{a}+\hat{a}^\dagger), \quad (4)$$

where $\hat{a}$ is the annihilation operator of the photonic cavity mode.

This leads to the usual coupling mechanism of a double quantum dot to a cavity mode which vanishes in case of a symmetric coupling ($g_L = g_R$), i.e., L and R orbitals couple equally to the cavity electric field. However, the superconductor gives rise to a coupling mechanism which works also in case of symmetric coupling. In order to evaluate it, one can still rely on the Schrieffer-Wolf transformation by including formally the operator $(\hat{a}+\hat{a}^\dagger)$ into the derivation and expanding in powers of g_L+g_R (since one assumes that $g_L - g_R \ll g_L + g_R$). To first order, this adds a term of the form

$$2\frac{\partial\delta t_b}{\partial\epsilon_\Sigma}(g_L+g_R)(\hat{a}+\hat{a}^\dagger). \quad (5)$$

It is important to note that although the above expression is in principle perturbative, it can in fact be much larger than the usual coupling term since in case of symmetric or nearly symmetric coupling ($g_L - g_R \ll g_L + g_R$). One can note that this "common-mode" coupling mechanism is in fact not restricted to our situation but would hold for any double quantum dot with a tunable barrier [25]. In our case, since the energy scale ruling the barrier tunability is the superconducting gap which is smaller than the semiconducting gaps of usual semiconducting materials, our tunability is very efficient. Finally, the effective Hamiltonian of our device in cavity, projected on the $\{|+\rangle, |-\rangle\}$ states reads as $\hat{H}_{\mathrm{eff,c}} = \hat{H}_{\mathrm{eff}} + \hbar\,\omega_{\mathrm{cav}}\,\hat{a}^\dagger\,\hat{a} + \hat{H}_{\mathrm{Baths}} + \hbar\tilde{g}(|+\rangle\langle -| + |-\rangle\langle +|)(\hat{a}+\hat{a}^\dagger)$ with the following coupling strength:

$$\tilde{g} \approx (g_L-g_R)\frac{2t_b}{\sqrt{\epsilon_\delta^2+4t_b^2}} + (g_L+g_R)\frac{4t_b}{\sqrt{\epsilon_\delta^2+4t_b^2}}\frac{\Gamma_{SR}-\Gamma_{SL}}{\Delta}\frac{\epsilon_\Sigma}{\Delta} - (g_L+g_R)\pi\frac{t_{eh}^0}{\Delta}\frac{2\epsilon}{\sqrt{\epsilon_\delta^2+4t_b^2}}. \quad (6)$$

The above equation contains three different terms: the first is the usual coupling term between a double-quantum-dot bonding/antibonding transition and a microwave cavity which needs to have asymmetric g_L and g_R. The second term corresponds to the fact that the superconductor renormalizes the energy levels of each dot with a strength proportional to each tunnel coupling $\Gamma_{SL(R)}$. It corresponds to an indirect Cooper-pair-assisted tunneling modulation between the two dots. The last term arises from the direct modulation of the Cooper-pair-assisted tunneling between the two dots by the cavity photons. The two last terms only exist in the presence of a superconductor. In the next section, we will illustrate with experimental values that the "common-mode" coupling mechanism can yield a sizable electron-photon coupling strength.

V. RESONANT INTERACTION BETWEEN THE HYBRID DOUBLE QUANTUM DOT AND THE CAVITY

The interaction between our hybrid double quantum dot and the cavity photons is conveniently probed by measuring the microwave signal transmitted through the cavity. Figures 3(a) and 3(b) [resp. 3(c) and 3(d)] display the phase

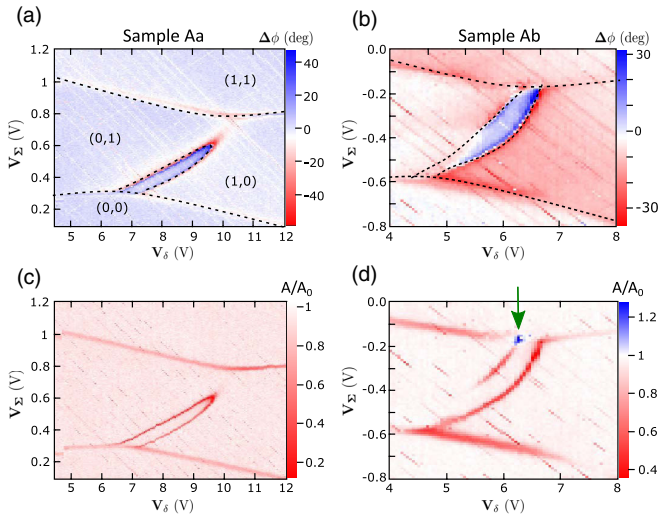

FIG. 3. (a), (b) [resp. (c), (d)] Microwave phase contrasts (resp. amplitude) maps at the bare resonator frequency f_c for sample A with two different tunings Aa and Ab as a function of the gate voltages. The charge occupation (i,j) of the double dot is indicated in (a). The sign changes demonstrate resonant interaction between the hybrid double quantum dot and the cavity photons. The elongated 0-phase line demonstrates the dependence of hopping with ϵ_Σ. The black dashed lines were obtained from theoretical expressions for the conditions $\omega_{\rm cav} = \omega_{S-{\rm DQD}}$ and $E_N = E_{N+1}$ with parameters given in the main text. In (d), the blue dot indicated by a green arrow is the sign of photon gain.

(resp. amplitude) contrasts for sample A with two different tunings (samples Aa and Ab). The avoided crossing lines are characteristic of a double-dot stability diagram and correspond to tunneling between the dots and the leads. We focus now on the most striking features, which lie within the area delimited by the avoided crossing. In Fig. 3(a), one observes a "crescent"-shaped 0-phase contour line with a phase shift spanning from $-40°$ to $+40°$. These features are similar for sample Ab presented in Fig. 3(b) although the "crescent" shape is cut by the electron lead transition lines. Similar to what has already been observed in double-quantum-dot setups [2,3,5,6], the sign change of the phase contrast signals a resonant interaction between a transition involving one or two electrons on the double dot and the cavity photons. Specifically, the cavity provides a "cut" of the dispersion relation of the circuit spectrum [6]. The contour line for $0°$ corresponds to the resonant condition $\omega_{\rm cav} \approx \omega_{S-{\rm DQD}}$, where $\omega_{\rm cav}$ is the cavity resonance frequency and $\omega_{S-{\rm DQD}}$ is the hybrid double-quantum-dot resonance frequency. However, in contrast with the standard double-quantum-dot response, the resonance contour line is not along the zero-detuning line $\epsilon_\delta = 0$ between the left (L) and the right (R) dots, but is distorted in the perpendicular direction. This means that the transition frequency of our circuit does not only depend on ϵ_δ, but also on the average energy of the two dots $\epsilon_\Sigma = \epsilon_L + \epsilon_R + U_m$. Qualitatively, this agrees with the theoretical expression for the transition frequency which we derived in Sec. III from a microscopic theory of our hybrid superconductor–double

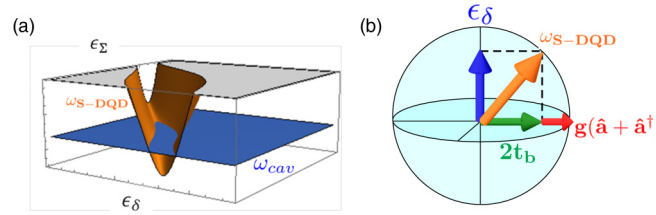

FIG. 4. (a) Diagram of the transition map of the hybrid double quantum dot intersecting with the cavity resonance frequency. This results in the phase contrast maps of Figs. 3(a) and 3(b). The axis are the orbital detuning ϵ_δ and the average orbital energy ϵ_Σ of the double dot. (b) Bloch sphere diagram depicting the active states of our hybrid double quantum dot and the tunable hopping strength. This symmetric coupling scheme is crucial for the strong electron-photon coupling.

quantum dot:

$$\hbar\omega_{S-{\rm DQD}} = \sqrt{\left(\epsilon_\delta^2 + 4t_b^2\right)Z(\epsilon_\delta,\epsilon_\Sigma)^2 + t(\epsilon_\delta,\epsilon_\Sigma)^2}. \quad (7)$$

The crescent shape of the transition line can be recast from the dependence of the functions Z and t on ϵ_δ and ϵ_Σ. As shown in Fig. 4(a), the transition frequency map expected from the theory as a function of ϵ_δ and ϵ_Σ, displayed in light brown, is cut by the blue plane at the cavity frequency. This results naturally in a crescent-shaped transition frequency contour line.

All these experimental signatures can be captured more quantitatively by an input-output formalism of the coupled equations of the cavity field in the semiclassical limit and the electronic degrees of freedom [1,17]. Specifically, the transmission t through the cavity reads as

$$t = \frac{\sqrt{\kappa_L\kappa_R}}{\omega - \omega_{\rm cav} - i\kappa/2 + g^2\chi_{\text{dot-dot}}(\omega) + g_c{}^2\chi_{\text{dot-lead}}(\omega)}, \quad (8)$$

where κ_L (resp. κ_R) is the photon loss rate through the left (resp. right) coupling ports of the resonator and κ is the total cavity photon loss rate. The bare cavity transition is modified by $\chi_{\text{dot-dot}}(\omega)$, which is the charge susceptibility for the internal transitions of the device and $\chi_{\text{dot-lead}}(\omega)$, which is the charge susceptibility involving electronic transitions from the dot to the leads (and vice versa). In our case, these susceptibilities read as

$$\chi_{\text{dot-dot}}(\omega) = \frac{1}{\omega - \omega_{S-{\rm DQD}} - i\Gamma/2}, \quad (9)$$

$$\chi_{\text{dot-lead}}(\omega) = \frac{1}{1 - i\omega/\gamma}\frac{\hbar}{4k_BT\cosh\left(\frac{E_N - E_{N+1}}{2k_BT}\right)}, \quad (10)$$

where Γ is the decoherence rate of the internal transition of the DQD and E_N is the energy of the DQD for N charges in total. The $\chi_{\text{dot-dot}}(\omega)$ susceptibility can give the strong electron-photon coupling if $g > \Gamma, \kappa$. This susceptibility yields a resonance in the transmission t when $\omega_{\rm cav} = \omega_{S\text{-DQD}}$ and allows to map the dispersion relation of our hybrid DQD. The $\chi_{\text{dot-lead}}(\omega)$ susceptibility is resonant when $E_N = E_{N+1}$ and allows to map the stability diagram of the DQD. We display in Figs. 3(a) and 3(b) the theory for the lines $\omega_{\rm cav} = \omega_{S\text{-DQD}}$ and $E_N = E_{N+1}$ in black dashed lines, using the following

parameters: aside from the measured value $\Delta/h = 37.5$ GHz [see Fig. 2(a)], we have for sample Aa $t_b/h = 6.3$ GHz, $\Gamma_{SR}/h = 400$ MHz, $\Gamma_{SL}/h = 900$ MHz, $t^0_{eh}/h = 400$ MHz, $U_L/h = 29$ GHz, $U_R/h = 71$ GHz, $U_m/h = 16$ GHz, and for sample Ab, we have $t_b/h = 5.5$ GHz, $\Gamma_{SR}/h = 330$ MHz, $\Gamma_{SL}/h = 900$ MHz, $t^0_{eh}/h = 350$ MHz, $U_L/h = 32$ GHz, $U_R/h = 42$ GHz, $U_m/h = 24$ GHz. The quantitative agreement with the $\omega_{\rm cav} = \omega_{S-{\rm DQD}}$ (internal) transition lines validates the low-energy spectrum of our device and is a direct observation of Cooper pair assisted tunneling between two quantum dots.

Noticeably, the renormalization of the hopping between the two dots is related to the Cooper pair splitting amplitude t^0_{eh} (see Sec. IV). Therefore, we can extract a value for $t^0_{eh}/h = 400$ MHz even without direct observation of Cooper pair splitting. Our measurement demonstrates that cavity photons can be used to probe very small energy scales, inaccessible to transport, related to superconducting proximity effect in quantum dots. Such a scheme could be generalized to superconducting hybrid structures with topological properties.

Additionally, it is important to notice that the dependence of $t(\epsilon_\delta, \epsilon_\Sigma)$ upon ϵ_Σ yields a light-matter coupling term for our device as shown in the previous section. This follows the original Loss and DiVincenzo proposal [25–28] and recent cavity-double-quantum-dot coupling proposals [36–38]. Our work provides an example of this common-mode coupling to a microwave cavity. Indeed, in the Bloch sphere representation of Fig. 4(b), the north and south poles are more along the detuning axis ϵ_δ and the light-matter coupling indicated by a red arrow is mainly along the tunnel coupling axis, in stark contrast with the usual case for double quantum dots [2,3,5–8], where it is along ϵ_δ. The electron-photon coupling strength is controlled by the sum $g_L + g_R$ which can easily be of the order of $2\pi \times 100$ MHz, as shown for example in Ref. [17], which is a large magnitude. Using expression (6) of Sec. IV with the circuit parameters of sample Aa given above, we get along the crescent contour a $\tilde{g}$ between $2\pi \times 1$ MHz ($\epsilon \approx 0$, $\epsilon_\Sigma \approx \Delta/2$) and $2\pi \times 4.7$ MHz ($\epsilon \approx 2t_b, \epsilon_\Sigma \approx 0$). This shows that the "common-mode" coupling mechanism can yield a sizable electron-photon coupling strength, even if it originates from second-order tunneling through the superconductor.

Finally, we briefly comment on an interesting feature of our light-matter interface which appears on Fig. 3(d). The amplitude map displays a "bright" spot, in blue, corresponding to photon gain (of about 1.3). Microwave photon emission from quantum-dot circuits was recently investigated in double quantum dots [39–42] and hybrid superconductor single quantum dot [17]. It is interesting to see that it also appears in our hybrid double-quantum-dot circuit, although we did not study this effect quantitatively. Qualitatively, it is consistent with having a coherent interface. In the next session, we show an even more striking consequence of the high cooperativity of our device, namely, the vacuum Rabi splitting of the cavity when it is brought into resonance with the DQD transition properly tuned.

VI. STRONG COUPLING

In the previous section, we have focused on characterizing our hybrid double-dot circuit, using the microwave resonator as a spectroscopic probe. However, looking at the large phase

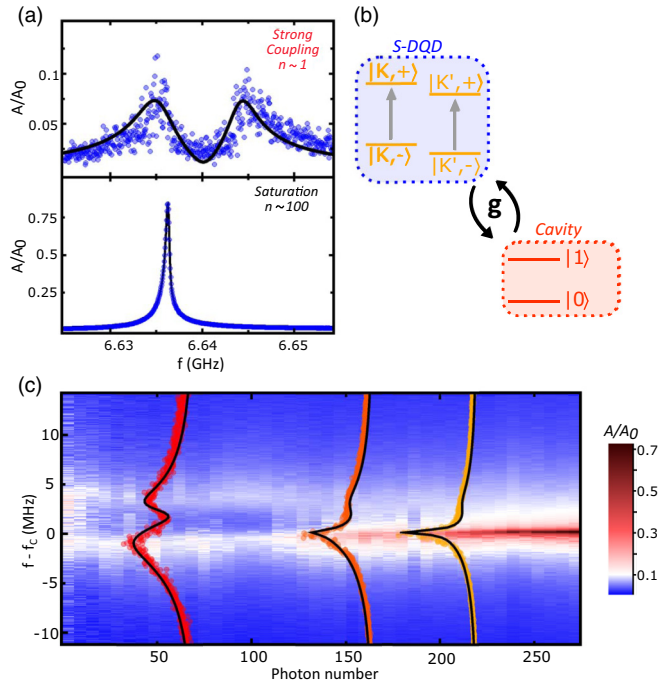

FIG. 5. (a) Top panel: vacuum Rabi splitting for sample B with n ∼ 1 photon. Bottom panel: saturation of the mode splitting for a large number of photons. The open blue circles are the data points and the black solid line is the theory. (b) Level structures explaining the strong coupling and its power dependence. The K, K' labels indicate the valley degree of freedom arising from the band structure of carbon nanotubes. (c) Power dependence of the mode splitting showing the gradual saturation of the coherent transition. Each cut can be fitted using the fully quantum light-matter interaction theory (QUTIP).

and amplitude contrasts measured in Fig. 3, one can wonder what happens to the cavity spectrum when the cavity is resonant with the DQD circuit transition. We tune the double-dot gate voltages to the point of maximum phase contrast and there, we measure the resonator transmission at a function of frequency (supplementary data in Appendix A). The top panel of Fig. 5(a) shows the result of the measurement for sample B, for which we measured the strongest effect. We observe a splitting of the order of 10 MHz in the cavity resonance for an average number of photons $\overline{n}$ of about 1. This observation persists down to the lowest input power which corresponds to $\overline{n} \ll 1$. This is the hallmark of a vacuum Rabi splitting which indicates the strong coupling between our hybrid double quantum dot and the microwave cavity photons. The fact that we observe this splitting implies that the coupling strength g between the circuit transition and the cavity is larger than half the linewidth of the cavity $\kappa/2$ and half the linewidth of the double-quantum-dot transition involved $\Gamma/2$. The intrinsic linewidth of the cavity can be directly measured from the transmission spectrum when the double dot is detuned and is $\kappa/2\pi = 0.5$ MHz. Therefore, the linewidth of the double-dot transition can be inferred from the linewidth of each peak observed in Fig. 5(a), of about 3 MHz. For the simplest case of a single transition [9], the linewidth is equal to $(\Gamma/2\pi + \kappa/2\pi)/2$. This would lead to

TABLE I. Summary of parameters used in the two-transition modeling. κ and f_c are, respectively, the decay rate and the resonance frequency of the cavity. g_i, f_i, $\Gamma_{\varphi,i}$, and γ_i are, respectively, the coupling strength, the frequency, the dephasing rate, and the decay rate of transition $i \in \{K, K'\}$.

	$\kappa/2\pi$ (MHz)	f_c (GHz)	$g_K/2\pi$ (MHz)	f_K (GHz)	$\Gamma_{\varphi,K}/2\pi$ (MHz)	$\gamma_K/2\pi$ (MHz)	$g_{K'}/2\pi$ (MHz)	$f_{K'}$ (GHz)	$\Gamma_{\varphi,K'}/2\pi$ (MHz)	$\gamma_{K'}/2\pi$ (MHz)
Fig. 5(a)	0.57	6.6364	4.6	6.6405	0	2	16.8	6.586	0	100
Fig. 5(c)	0.42	6.6362	1.4	6.6378	0.4	0.8	4.2	6.636	5	6

$\Gamma/2\pi \sim 5.5$ MHz. In order to account quantitatively for the observed transmission spectrum (and in particular for the very low transmission maximum), we can rely on a two-transition scheme (one very coherent, one less coherent). Using a modeling based on two independent transitions depicted in Fig. 5(b), we are able to fit the data using a fully quantum numerical code (QUTIP, see Appendix C for details). The use of two transitions anticipates on the existence of a K/K' valley degree of freedom commonly observed in nanotubes. We use the following parameters: $g_K = 2\pi \times 4.6$ MHz, $\Gamma_K = 2\pi \times 2$ MHz, $g_{K'} = 2\pi \times 16.8$ MHz, $\Gamma_{K'} = 2\pi \times 100$ MHz (see Table I for all the parameters). It is important to note here that the K/K' valleys are in general coupled by weak disorder in carbon nanotubes [43]. Therefore, the K/K' eigenstates correspond to linear combinations of the original (degenerate) valley states. Their coupling to the field and decoherence rates is therefore different in general. As one can see in Table I, a low coupling strength is accompanied by a low decoherence rate ("K" mode) whereas a large coupling strength is accompanied by a large decoherence rate ("K"' mode).

As expected for a few-level system, we are able to saturate the transitions and to recover the bare transmission of the cavity by injecting a large number of photons inside the cavity. In the present case, this saturation occurs for $\overline{n} \approx 100$. As shown in Fig. 5(c), there is a continuous evolution from the vacuum Rabi splitting to a single off-centered Lorentzian peak from $\overline{n} \approx 0.1$ to $\overline{n} \approx 300$. Such a peculiar saturation is well reproduced by the QUTIP numerical simulation and arises from the two-transition structure mentioned above. Note that the splitting at low power is slightly smaller (about 6 MHz) in Fig. 5(c) than in Fig. 5(a) because this measurement was done for a different working point of our device.

Reaching the strong coupling regime with an excitation which is primarily chargelike is nontrivial and has been the main challenge of the mesoscopic cQED community for years until recently. The main limitation of all the charge-qubit-like setups in cavity is the linewidth of the double-dot transition which is typically reported to be at least in the few 100 MHz range [2,3,5]. One important decoherence source explaining such a large linewidth is the background charge noise. One can think of several strategies to overcome this difficulty. One possible path is to reduce the charge noise in the material. Recently, this idea was successfully implemented by Mi *et al.* in a SiGe-based two-dimensional electron gas double quantum dot [8], with a linewidth $\Gamma/2\pi = 2.6$ MHz lower than the coupling $g/2\pi = 13.4$ MHz. An alternative strategy to reach the strong coupling regime despite the presence of large charge noise was demonstrated by Stockklauser *et al.* [7]: by using a squid array resonator, the electron-photon coupling was increased to $g/2\pi = 238$ MHz, which exceeds the DQD charge-qubit linewidth $\Gamma/2\pi = 93$ MHz. Our ability to reach the strong coupling regime relies on a third approach, namely, reducing our qubit linewidth by reducing the device sensitivity to charge noise. In this scheme, our specific common-mode coupling mechanism plays a crucial role to keep a sufficient coupling strength. Now, we successively detail each of these two key ingredients.

In presence of the noise spectral density $S(f) = \langle \delta n^2 \rangle / f$, where f is the frequency, the dephasing rate Γ_φ of the double dot can be expressed as

$$\Gamma_\varphi \approx \frac{\partial \omega}{\partial \epsilon} E_C \sqrt{\langle \delta n^2 \rangle} + \frac{1}{2} \frac{\partial^2 \omega}{\partial \epsilon^2} {E_C}^2 \langle \delta n^2 \rangle + \cdots \tag{11}$$

which is strongly influenced by the charging energy $E_C \sim e^2/C_\Sigma$, where C_Σ is the total capacitance of the device [5,44–46]. The expression of Γ_φ takes the above simple form only if the transition frequency ω depends on a single parameter ϵ. This is the case for the standard double-quantum-dot charge-qubit transition ω_{DQD}, which dispersion relation is governed by ϵ_δ. In our case, the expression of Γ_φ is more complex since it involves all the derivatives of the transition $\omega_{S\text{–}\mathrm{DQD}}$, with respect to its control parameters ϵ_δ and ϵ_Σ. Nevertheless, its dependence as a function of the total charging energy and the transition frequency derivatives remains qualitatively the same. The points where all the first-order derivatives vanish are called sweet spots [36–38] because the double dot is insensitive at first order to charge noise. The usual method to reduce Γ_φ is therefore to operate the system close to a sweet spot which implies that only the second-order terms are present in the expression of Γ_φ. To reduce the second-order term at constant noise density and without engineering the dispersion relation [47], it is *a priori* very efficient to go towards small charging energy, in analogy with the transmon qubit [45]. The charging energy of samples A and B can simply be read off from the transport stability diagram which is shown in Fig. 2(a) for sample A. Due to the fork-shaped top gates that increase the capacitance to the ground, our charging energy is 2 meV, about 10 times smaller than what we find typically for similar devices with a conventional top-gate setting [5,6]. Since $\Gamma_\varphi/2\pi \approx 400$ MHz in those conventional settings, a reduction of 10 of E_C is expected to reduce Γ_φ by a factor of 100, i.e., $\Gamma_\varphi/2\pi \approx 4$ MHz, which is consistent with the order of magnitude of $\Gamma/2\pi \sim$ few MHz inferred from the cavity spectroscopy of Fig. 5(a).

Importantly, this reduction of E_C also implies a decrease of the lever arm between the orbital energies ϵ_L, ϵ_R of the dots and the cavity potentials. The coupling of photons through the variable ϵ_δ used in former experiments [2,3,5,6] thus becomes too small to be exploited. However, our hopping $t(\epsilon_\delta, \epsilon_\Sigma)$ is tunable with the parameter ϵ_Σ, which is naturally

more strongly coupled to the cavity potential than ϵ_δ. This compensates the decrease of E_C and gives us a large charge-photon coupling strength of about $2\pi \times 10$ MHz which allows us to reach the strong coupling regime.

VII. CONCLUSION

We have presented an experimental study of a hybrid superconductor–double quantum dot in a microwave cavity. The resonant interaction between cavity photons and a charge-qubit-like transition of our circuit reveals a peculiar dispersion map as a function of the dot gate voltages. We are able to interpret our data by theoretically deriving the device energy level structure, which is dressed by cotunneling processes between the left and the right dots induced by the superconductor. This is a direct observation of Cooper-pair-assisted cotunneling in a double quantum dot. Due to its relation to the Cooper pair splitting, we are able to extract a value for $t_{eh}^0/h \sim$ 400 MHz, which is inaccessible to transport measurements. A natural perspective of our work is to use the theoretical and experimental tools developed here to study the same type of device with a more transparent superconducting contact, i.e. with larger t_{eh}^0. In principle, such a regime would allow to study the physics of Cooper pair splitting more directly [18,19]. The same methods could also be instrumental to the study of Majorana bound states through microwave cavities [48,49].

Importantly, our qubit design demonstrates a way of reaching the strong electron-photon coupling based on a tunable hopping barrier and a low charging energy. These ingredients are very generic and could be used in many other setups [36–38]. In our case, the tunable hopping is due to the use of a hybrid superconductor double-quantum-dot setup, thanks to superconductor-induced cotunneling processes. However, using local gates, one could also engineer a direct electrostatic control over the hopping strength. Our findings open the path for entanglement of individual electron states [50] and teleportation of electronic entanglement over macroscopic distances.

A preliminary version of this work was communicated at the conference ICPS (August 2016) in Beijing [51].

ACKNOWLEDGMENTS

We are indebted with J. M. Raimond, C. Schönenberger, and A. Baumgartner for discussions. We acknowledge technical support from J. Palomo, M. Rosticher, A. Denis, P. Pace, and the ENS mechanical workshop. The devices have been made within the consortium Salle Blanche Paris Centre. This work is supported by European Research Council Starting Grant CIRQYS.

APPENDIX A: EXPERIMENTAL DETAILS

1. Sample fabrication and measurement setup

The sample fabrication process is the following. A 150-nm-thick Nb film is first evaporated on a thermal silicon oxide (500 nm)/high resistivity (10 $k\Omega$ cm) silicon substrate at rate of 1 nm/s and a pressure of 10^{-9} mbar. The cavity is made subsequently using photolithography combined with reactive ion etching (SF6 process). Carbon nanotubes are grown with chemical vapor deposition technique (CVD) at about 900 °C using a methane process on a separate quartz substrate and stamped inside the cavity. The nanotubes are then localized. The fork top gate oxide is made using three evaporation steps of Al (2 nm) followed each by an oxidation of 10 min under an O_2 pressure of 1 mbar. The Alox is covered by a Al(40 nm)/Pd(20 nm) layer. The nanotube is contacted with a central Pd(4 nm)/Al(80 nm) finger and two Pd(70 nm) outer electrodes.

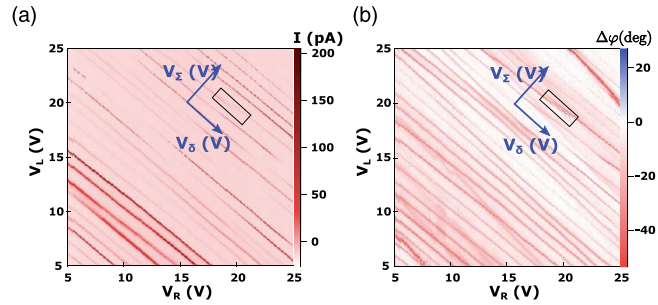

FIG. 6. Large-scale characterization of sample A in the V_L-V_R plane. Current (a) and phase contrast (b) color maps as a function of the two side gate voltages V_L and V_R for sample A. The black rectangle indicates the area Aa under study in the main text. The blue axis show the relative orientation of the $V_\Sigma - V_\delta$ frame, which was used to measure all data presented in this paper for sample A. Note that for clarity the frame origin chosen at ($V_L = 20$ V ; $V_R = 20$ V) is shifted on the figure.

The dc measurements are carried out using standard lock-in detection techniques with a modulation frequency of 137 Hz and an amplitude of 10 μV. The base temperature of the experiment is 18 mK. The microwave measurements are carried out using room-temperature microwave amplifiers and a cryogenic amplifier (noise temperature about 5 K) with a total gain of about 90 dB. We measure both quadratures of the transmitted microwave signal using an I-Q mixer and low frequency modulation at 2.7 kHz.

2. Supplementary data: Double-dot stability diagram

Figure 6 shows current (a) and phase contrast (b) color maps as a function of the two side gate voltages V_L and V_R for sample A. For this measurement, the two normal electrodes were biased with equal voltages with respect to the superconducting electrode, where the current was measured. The zone labeled Aa in the paper is enclosed in a black rectangle. The lines avoided crossing in the current and the sign change of the phase contrast are indicative of a local double-dot behavior, where an internal transition is resonant with the cavity. To better resolve the features of this area in a shorter time, further measurements were carried out using the orthonormal frame $V_\Sigma - V_\delta$, which results from a 42° clockwise rotation of the original frame $V_L - V_R$ and a translation of the origin to ($V_L = 20$ V ; $V_R = 20$ V).

Such a resolved characterization of sample Aa resonant area is presented on Figs. 3(a), 3(c), and 7 showing the simultaneously measured transmitted cavity signal phase and amplitude and differential conductances, respectively. Figure 7

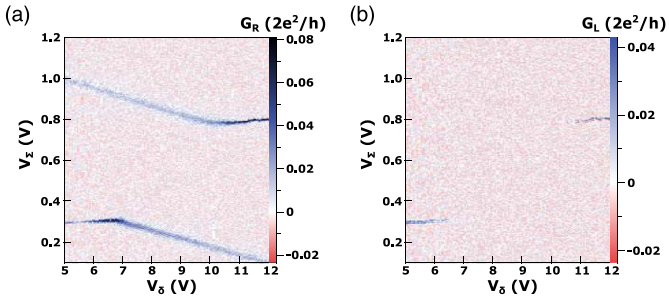

FIG. 7. Double-dot stability diagram in transport measurement for sample A. Right (a) and left (b) differential conductance maps in the rotated gate-gate frame V_Σ-V_δ with a bias voltage $V_S = -0.16$ mV applied to the superconducting electrode. This measurement is simultaneous with the cavity transmission measurement presented in Fig. 3(a) for the phase and 3(c) for the amplitude.

shows a clear avoided crossing in transport measurements, which means that sample A locally behaves as a double quantum dot. The transport characterization of sample B does not show any measurable currents above our noise level $\sim$1 pA.

3. Supplementary data: Hybridization of cavity-dot system

Figure 8 illustrates how the photonic and electronic degrees of freedom hybridize when the gates of the devices are tuned into the strong coupling region. Figure 8(b) [resp. 8(d)] displays for sample A (resp. sample B) the amplitude of the microwave transmitted signal as a function of the detuning f-f_c between probe frequency f and cavity bare resonance frequency f_c and the gate voltage V_δ (resp. V_L). The latter parameter range together with the constant value of V_Σ (resp. V_R) where the measurement is performed are indicated

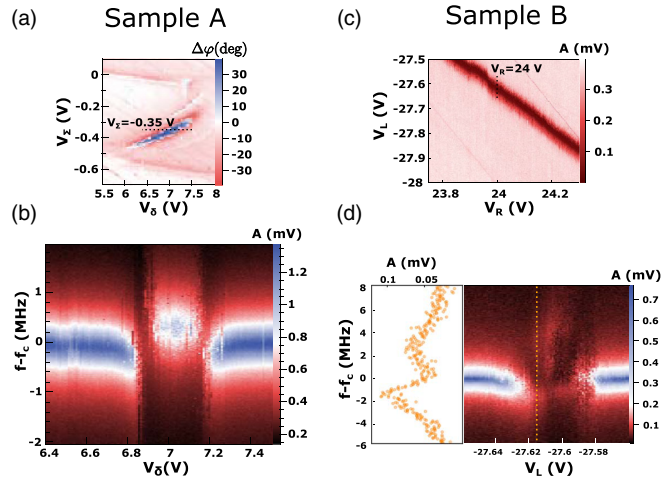

FIG. 8. Phase map as a function of V_δ and V_Σ for sample A. The black dotted line indicates for which parameters the cavity spectra are shown on (b). (b) Cavity spectrum as a function V_δ for sample A. (c) Phase map as a function of V_L and V_Σ for sample B. The black dotted line indicates for which parameters the cavity spectra are shown on (d). (d) Cavity spectrum as a function V_L for sample B. The orange vertical dotted line shows the cut along which the spectrum showing the Rabi splitting on the left has been taken.

by a black dashed line on Fig. 8(a) [resp. 8(b)]. Changing the dot gate voltage tunes the quantum-dot circuit transition frequency in and out of resonance with the cavity: the resonance condition is accompanied by large distortions in the cavity transmission demonstrating a strong coupling between photonic and electronic degrees of freedom.

APPENDIX B: THEORY OF THE LOW-ENERGY SPECTRUM OF A COOPER SPLITTER

This appendix is a more detailed version of the derivation of the low-energy spectrum of a hybrid superconductor double quantum dot given in Sec. III of the main text. The Hamiltonian of a double dot with a central superconducting lead can be written as $H = H_0 + H_{S\text{-DQD}}$, where $H_0 = H_{\text{DQD}} + H_S$ is the sum of the individual Hamiltonians and $H_{S\text{-DQD}}$ describes the coupling between them. Let us recall the explicit expressions for each term:

$$H_{\text{DQD}} = \epsilon_L\,\hat{n}_L + \epsilon_R\,\hat{n}_R + t_b(c^\dagger_{L\uparrow}c_{R\uparrow} + c^\dagger_{L\downarrow}c_{R\downarrow}) + \text{H.c.} + U_m\hat{n}_L\hat{n}_R + \tfrac{1}{2}U_L\hat{n}_L(\hat{n}_L - 1) + \tfrac{1}{2}U_R\hat{n}_R(\hat{n}_R - 1), \tag{B1}$$

$$H_S = \sum_{k\sigma} E_k \gamma^\dagger_{k\sigma}\gamma_{k\sigma}, \tag{B2}$$

$$H_{S\text{–DQD}} = \sum_{k\sigma, i\in\{L,R\}} t_i^* \mathcal{A}^i_{k\sigma} c^\dagger_{j\sigma} + \text{H.c.}, \tag{B3}$$

where $t_i \equiv \sqrt{\Gamma_{Si}}$ and $\mathcal{A}^j_{k\sigma} = \sum_{k\sigma, j\in\{L,R\}} e^{ik.r_j}u_k\gamma_{k\sigma} + \sigma e^{-ik.r_j}v_{-k}\gamma^\dagger_{k\bar{\sigma}}$ with u_k and v_k as conventionally defined in the BCS theory.

The main step of the derivation is to write an effective Hamiltonian to second order in the tunnel couplings t_i of the superconductor to the two dots using a Schrieffer-Wolf transformation, also called adiabatic elimination in atomic physics [12,35]. The idea is to find a unitary transformation which cancels the tunneling term up to second order in tunneling. The effective Hamiltonian reads as

$$\hat{H}_{\text{eff}} = e^{-S}\hat{H}e^{S} \approx \hat{H} - [S,\hat{H}] + \tfrac{1}{2}[S,[S,\hat{H}]] + \cdots.$$

If S is constructed such that $[S,\hat{H}_0] = \hat{H}_{S\text{–DQD}}$, the effective Hamiltonian becomes

$$\hat{H}_{\text{eff}} \approx \hat{H}_0 - \tfrac{1}{2}[S,\hat{H}_{S\text{–DQD}}].$$

One seeks for the operator S in the following form:

$$S = \sum_{\substack{k\sigma \\ j\,\in\,\{L,R\}}} \gamma_{k\sigma}X^j_{k\sigma} - \text{H.c.}$$

The constraints for the operator S can be fulfilled if $X^j_{k\sigma}$ has the following matrix elements:

$$\langle l|\,X^j_{k\sigma}\,|m\rangle = \frac{-t_j\sigma e^{ik\cdot r_j}v^*_{-k}\langle l|\,d_{j\sigma}\,|m\rangle + t^*_j e^{ik.r_j}u_k\langle l|d^\dagger_{j\sigma}|m\rangle}{E_k + E_m - E_l}. \tag{B4}$$

This allows us to calculate explicit expressions of the double-quantum-dot effective Hamiltonian by using the ground state of the superconductor in the initial and final states and states in which one quasiparticle is excited in the superconductor as intermediate states. In the bonding/antibonding basis, we get, setting $\delta r = r_L - r_R$ the distance between tunneling to left and right dots:

$$\langle +|\,[S, \hat{H}_{S\text{–DQD}}]\,|-\rangle = \sum_k |u_k|^2 \left(\frac{1}{E_k - E_+} + \frac{1}{E_k - E_-}\right)\{-uv(|t_L|^2 - |t_R|^2) + t_L^* t_R e^{ik\cdot\delta r}u^2 - t_R^* t_L e^{-ik\cdot\delta r}v^2\}$$
$$- |v_{-k}|^2 \left(\frac{1}{E_k - E_+ + \epsilon_\Sigma} + \frac{1}{E_k - E_- + \epsilon_\Sigma}\right)\{uv(|t_L|^2 - |t_R|^2) + t_L^* t_R e^{-ik\cdot\delta r}u^2 - t_R^* t_L e^{ik\cdot\delta r}v^2\}. \quad \text{(B5)}$$

We get similar expressions for $\langle +|\,[S, \hat{H}_{S\text{–DQD}}]\,|+\rangle$ and $\langle -|\,[S, \hat{H}_{S\text{–DQD}}]\,|-\rangle$. In order to obtain useful analytical expressions, we use the following identities, taking the 1D limit similarly to Ref. [52], assuming the tunnel coupling t_i is real and setting $t_i = \sqrt{\Gamma_{Si}}$, to second order in $\frac{\epsilon}{\Delta}$ where ϵ is the energy of the state:

$$t_i t_j \sum_k u_k v_{-k} \frac{e^{ik\cdot\delta r}}{E_k + \epsilon} \begin{cases} = \sqrt{\Gamma_{Si}\Gamma_{Sj}}\left(\pi - \frac{2\epsilon}{\Delta} + \frac{\pi}{2}\frac{\epsilon^2}{\Delta^2} + \cdots\right) & \text{for} \quad \delta r = 0, \\ = \pi\sqrt{\Gamma_{Si}\Gamma_{Sj}}\cos k_F \delta r\; e^{-\delta r/\xi_0}\left(1 - \sqrt{\frac{2|\delta r|}{\pi\xi_0}}\frac{\epsilon}{\Delta} + \frac{|\delta r|}{2\xi_0}\frac{\epsilon^2}{\Delta^2} + \cdots\right) & \text{for} \quad \delta r \gg \xi_0, \end{cases} \quad \text{(B6)}$$

$$t_i t_j \sum_k |u_k|^2 \frac{e^{ik\cdot\delta r}}{E_k + \epsilon} \begin{cases} = \sqrt{\Gamma_{Si}\Gamma_{Sj}}\left(Ln\frac{2\hbar\omega_D}{\Delta} - \frac{\pi}{2}\frac{\epsilon}{\Delta} + \frac{\epsilon^2}{\Delta^2} + \cdots\right) & \text{for} \quad \delta r = 0, \\ = \pi\sqrt{\Gamma_{Si}\Gamma_{Sj}}\cos k_F \delta r\; e^{-\delta r/\xi_0}\left(\sqrt{\frac{\pi\xi_0}{2|\delta r|}} - \frac{\pi}{2}\frac{\epsilon}{\Delta} + \sqrt{\frac{\pi|\delta r|}{2\xi_0}}\frac{\epsilon^2}{\Delta^2} + \cdots\right) & \text{for} \quad \delta r \gg \xi_0, \end{cases} \quad \text{(B7)}$$

where ω_D is the Debye angular frequency used as a cutoff and Δ is the superconducting gap. It is interesting to note that $\sqrt{\Gamma_{SL}\Gamma_{SR}}\cos k_F \delta r\; e^{-\delta r/\xi_0}$ is the Cooper pair splitting amplitude which appears both here in the renormalization of the bonding/antibonding states as well as in the hybridization between the $|S\rangle$ and the $|0,0\rangle$. We note

$$t_{eh}^0 = \sqrt{\Gamma_{SL}\Gamma_{SR}}\cos k_F \delta r\; e^{-\delta r/\xi_0}. \quad \text{(B8)}$$

Projecting the effective Hamiltonian on the $\{|+\rangle, |-\rangle\}$, we get

$$\hat{H}_{\text{eff}} = (E_+ + \delta E_+)|+\rangle\langle +| + (E_- + \delta E_-)|-\rangle\langle -| + \delta t_b\,|+\rangle\langle -| + \delta t_b\,|-\rangle\langle +|, \quad \text{(B9)}$$

where the expressions for the perturbative elements close to the degeneracy line between (0,1)/(1,0) charge states are given in the main text.

APPENDIX C: VACUUM RABI SPLITTING POWER DEPENDENCE MODELING

In this appendix we present the modeling of the vacuum Rabi splittings shown in Figs. 5(a) and 5(c) of the main text. In both figures, a misalignment is visible between the center of the Rabi splitting peaks and the recovered coherent state at high power, whereas the spectral weight of the two peaks at low power remains the same. Such a misalignment can be accounted for by a two-transition structure depicted in Fig. 5(b). This contrasts with the case of a single electronic transition involved, where this shift would automatically be accompanied by asymmetric spectral weights on the two peaks.

We can account for this asymmetric splitting with respect to the coherent state peak at the cavity frequency recovered at high power, while keeping similar spectral weight on each peak, with the two-transition scheme depicted in Fig. 5(b). As an example, we give three different transmission spectra with their theoretical fit in Fig. 5(c). The sets of parameters used to reproduce all the transmission spectra are given in Table I. The photon number used in the model is 7 dB lower than the estimated experimental photon number used as x axis in Fig. 5(c).

In the Supplemental Material [53] we give the python code (using the QUTIP package) that calculates the reduced density matrix and the cavity transmission.

[1] Audrey Cottet, Matthieu C. Dartiailh, Matthieu M. Desjardins, Tino Cubaynes, Lauriane C. Contamin, Matthieu Delbecq, Jérémie J. Viennot, Laure E. Bruhat, Benoit Douçot, and Takis Kontos, Cavity QED with hybrid nanocircuits: From atomic-like physics to condensed matter phenomena, J. Phys.: Condens. Matter **29**, 433002 (2017).

[2] K. D. Petersson, L. W. McFaul, M. D. Schroer, M. Jung, J. M. Taylor, A. A. Houck, and J. R. Petta, Circuit quantum electrodynamics with a spin qubit, Nature (London) **490**, 380 (2012).

[3] T. Frey, P. J. Leek, M. Beck, J. Faist, A. Wallraff, K. Ensslin, T. Ihn, and M. Büttiker, Quantum dot admittance probed at microwave frequencies with an on-chip resonator, Phys. Rev. B **86**, 115303 (2012).

[4] J. Basset, D.-D. Jarausch, A. Stockklauser, T. Frey, C. Reichl, W. Wegscheider, T. M. Ihn, K. Ensslin, and A. Wallraff,

Single-electron double quantum dot dipole-coupled to a single photonic mode, Phys. Rev. B **88**, 125312 (2013).

[5] J. J. Viennot, M. R. Delbecq, M. C. Dartiailh, A. Cottet, and T. Kontos, Out-of-equilibrium charge dynamics in a hybrid circuit quantum electrodynamics architecture, Phys. Rev. B **89**, 165404 (2014).

[6] J. J. Viennot, M. C. Dartiailh, A. Cottet, and T. Kontos, Coherent coupling of a single spin to microwave cavity photons, Science **349**, 408 (2015).

[7] A. Stockklauser, P. Scarlino, J. V. Koski, S. Gasparinetti, C. K. Andersen, C. Reichl, W. Wegscheider, Th. Ihn, K. Ensslin, and A. Wallraff, Strong Coupling Cavity QED with Gate-Defined Double Quantum Dots Enabled by a High Impedance Resonator, Phys. Rev. X **7**, 011030 (2017).

[8] X. Mi, J. V. Cady, D. M. Zajac, P. W. Deelman, and J. R. Petta, Strong coupling of a single electron in silicon to a microwave photon, Science **355**, 156 (2017).

[9] A. Wallraff, D. I. Schuster, A. Blais, L. Frunzio, R.-S. Huang, J. Majer, S. Kumar, S. M. Girvin, and R. J. Schoelkopf, Circuit quantum electrodynamics: coherent coupling of a single photon to a cooper pair box, Nature (London) **431**, 162 (2004).

[10] S. M. Albrecht, A. P. Higginbotham, M. Madsen, F. Kuemmeth, T. S. Jespersen, J. Nygård, P. Krogstrup, and C. M. Marcus, Exponential protection of zero modes in Majorana islands, Nature (London) **531**, 206 (2016).

[11] V. Mourik, K. Zuo, S. M. Frolov, S. R. Plissard, E. P. A. M. Bakkers, and L. P. Kouwenhoven, Signatures of Majorana fermions in hybrid superconductor-semiconductor nanowire devices, Science **336**, 1003 (2012).

[12] P. Recher, E. V. Sukhorukov, and D. Loss, Andreev tunneling, Coulomb blockade, and resonant transport of nonlocal spin-entangled electrons, Phys. Rev. B **63**, 165314 (2001).

[13] P. Recher and D. Loss, Superconductor coupled to two Luttinger liquids as an entangler for electron spins, Phys. Rev. B **65**, 165327 (2002).

[14] L. Hofstetter, S. Csonka, J. Nygård, and C. Schönenberger, Cooper pair splitter realized in a two-quantum-dot Y-junction, Nature (London) **461**, 960 (2009).

[15] L. G. Herrmann, F. Portier, P. Roche, A. L. Yeyati, T. Kontos, and C. Strunk, Carbon Nanotubes as Cooper-Pair Beam Splitters, Phys. Rev. Lett. **104**, 026801 (2010).

[16] C. Janvier, L. Tosi, L. Bretheau, C. O. Girit, M. Stern, P. Bertet, P. Joyez, D. Vion, D. Esteve, M. F. Goffman, H. Pothier, and C. Urbina, Coherent manipulation of Andreev states in superconducting atomic contacts, Science **349**, 1199 (2015).

[17] L. E. Bruhat, J. J. Viennot, M. C. Dartiailh, M. M. Desjardins, T. Kontos, and A. Cottet, Cavity Photons as a Probe for Charge Relaxation Resistance and Photon Emission in a Quantum Dot Coupled to Normal and Superconducting Continua, Phys. Rev. X **6**, 021014 (2016).

[18] A. Cottet, T. Kontos, and A. L. Yeyati, Subradiant Split Cooper Pairs, Phys. Rev. Lett. **108**, 166803 (2012).

[19] A. Cottet, Probing coherent Cooper pair splitting with cavity photons, Phys. Rev. B **90**, 125139 (2014).

[20] O. Sauret, D. Feinberg, and Thierry Martin, Quantum master equations for the superconductor-quantum dot entangler, Phys. Rev. B **70**, 245313 (2004).

[21] O. Sauret, Thierry Martin, and D. Feinberg, Spin-current noise and Bell inequalities in a realistic superconductor-quantum dot entangler, Phys. Rev. B **72**, 024544 (2005).

[22] D. Chevallier, J. Rech, T. Jonckheere, and T. Martin, Current and noise correlations in a double-dot Cooper-pair beam splitter, Phys. Rev. B **83**, 125421 (2011).

[23] L. Hofstetter, S. Csonka, A. Baumgartner, G. Fülöp, S. d'Hollosy, J. Nygård, and C. Schönenberger, Finite-Bias Cooper Pair Splitting, Phys. Rev. Lett. **107**, 136801 (2011).

[24] Z. B. Tan, D. Cox, T. Nieminen, P. Lähteenmäki, D. Golubev, G. B. Lesovik, and P. J. Hakonen, Cooper Pair Splitting by Means of Graphene Quantum Dots, Phys. Rev. Lett. **114**, 096602 (2015).

[25] D. Loss and D. P. DiVincenzo, Quantum computation with quantum dots, Phys. Rev. A **57**, 120 (1998).

[26] B. Bertrand, H. Flentje, S. Takada, M. Yamamoto, S. Tarucha, A. Ludwig, A. D. Wieck, C. Bäuerle, and T. Meunier, Quantum Manipulation of Two-Electron Spin States in Isolated Double Quantum Dots, Phys. Rev. Lett. **115**, 096801 (2015).

[27] F. Martins, F. K. Malinowski, P. D. Nissen, E. Barnes, S. Fallahi, G. C. Gardner, M. J. Manfra, C. M. Marcus, and F. Kuemmeth, Noise Suppression Using Symmetric Exchange Gates in Spin Qubits, Phys. Rev. Lett. **116**, 116801 (2016).

[28] M. D. Reed, B. M. Maune, R. W. Andrews, M. G. Borselli, K. Eng, M. P. Jura, A. A. Kiselev, T. D. Ladd, S. T. Merkel, I. Milosavljevic, E. J. Pritchett, M. T. Rakher, R. S. Ross, A. E. Schmitz, A. Smith, J. A. Wright, M. F. Gyure, and A. T. Hunter, Reduced Sensitivity to Charge Noise in Semiconductor Spin Qubits via Symmetric Operation, Phys. Rev. Lett. **116**, 110402 (2016).

[29] X. Mi, M. Benito, S. Putz, D. M. Zajac, J. M. Taylor, G. Burkard, and J. R. Petta, A coherent spin-photon interface in silicon, Nature (London) **555**, 599 (2018).

[30] N. Samkharadze, G. Zheng, N. Kalhor, D. Brousse, A. Sammak, U. C. Mendes, A. Blais, G. Scappucci, and L. M. K. Vandersypen, Strong spin-photon coupling in silicon, Science **359**, 1123 (2018).

[31] A. J. Landig, J. V. Koski, P. Scarlino, U. C. Mendes, A. Blais, C. Reichl, W. Wegscheider, A. Wallraff, K. Ensslin, and T. Ihn, Coherent spin-qubit photon coupling, Nature (London) **560**, 179 (2018).

[32] J. J. Viennot, J. Palomo, and T. Kontos, Stamping single wall nanotubes for circuit quantum electrodynamics, Appl. Phys. Lett. **104**, 113108 (2014).

[33] M. R. Delbecq, V. Schmitt, F. D. Parmentier, N. Roch, J. J. Viennot, G. Fève, B. Huard, C. Mora, A. Cottet, and T. Kontos, Coupling a Quantum Dot, Fermionic Leads, and a Microwave Cavity on a Chip, Phys. Rev. Lett. **107**, 256804 (2011).

[34] J. Eldridge, M. G. Pala, M. Governale, and J. König, Superconducting proximity effect in interacting double-dot systems, Phys. Rev. B **82**, 184507 (2010).

[35] S. E. Nigg, R. P. Tiwari, S. Walter, and Thomas L. Schmidt, Detecting nonlocal Cooper pair entanglement by optical Bell inequality violation, Phys. Rev. B **91**, 094516 (2015).

[36] M. Friesen, J. Ghosh, M. A. Eriksson, and S. N. Coppersmith, A decoherence-free subspace in a charge quadrupole qubit, Nat. Commun. **8**, 15923 (2017).

[37] V. Srinivasa, J. M. Taylor, and C. Tahan, Entangling distant resonant exchange qubits via circuit quantum electrodynamics, Phys. Rev. B **94**, 205421 (2016).

[38] M. Russ and G. Burkard, Long distance coupling of resonant exchange qubits, Phys. Rev. B **92**, 205412 (2015).

[39] J. Stehlik, Y.-Y. Liu, C. Eichler, T. R. Hartke, X. Mi, M. J. Gullans, J. M. Taylor, and J. R. Petta, Double Quantum Dot Floquet Gain Medium, Phys. Rev. X **6**, 041027 (2016).

[40] Y.-Y. Liu, J. Stehlik, M. J. Gullans, J. M. Taylor, and J. R. Petta, Injection locking of a semiconductor double-quantum-dot micromaser, Phys. Rev. A **92**, 053802 (2015).

[41] A. Stockklauser, V. F. Maisi, J. Basset, K. Cujia, C. Reichl, W. Wegscheider, T. Ihn, A. Wallraff, and K. Ensslin, Microwave Emission from Hybridized States in a Semiconductor Charge Qubit, Phys. Rev. Lett. **115**, 046802 (2015).

[42] Y.-Y. Liu, J. Stehlik, C. Eichler, M. J. Gullans, J. M. Taylor, and J. R. Petta, Semiconductor double quantum dot micromaser, Science **347**, 285 (2015).

[43] E. A. Laird, F. Kuemmeth, G. A. Steele, K. Grove-Rasmussen, J. Nygård, K. Flensberg, and L. P. Kouwenhoven, Quantum transport in carbon nanotubes, Rev. Mod. Phys. **87**, 703 (2015).

[44] A. Cottet, D. Vion, A. Aassime, P. Joyez, D. Esteve, and M. H. Devoret, Implementation of a combined charge-phase quantum bit in a superconducting circuit, Phys. C Supercond. **367**, 197 (2002).

[45] J. Koch, T. M. Yu, J. Gambetta, A. A. Houck, D. I. Schuster, J. Majer, A. Blais, M. H. Devoret, S. M. Girvin, and R. J. Schoelkopf, Charge-insensitive qubit design derived from the Cooper pair box, Phys. Rev. A **76**, 042319 (2007).

[46] Audrey Cottet and Takis Kontos, Spin Quantum Bit with Ferromagnetic Contacts for Circuit QED, Phys. Rev. Lett. **105**, 160502 (2010).

[47] M. Russ, F. Ginzel, and G. Burkard, Coupling of three-spin qubits to their electric environment, Phys. Rev. B **94**, 165411 (2016).

[48] A. Cottet, T. Kontos, and B. Douçot, Squeezing light with Majorana fermions, Phys. Rev. B **88**, 195415 (2013).

[49] M. C. Dartiailh, T. Kontos, B. Douçot, and A. Cottet, Direct Cavity Detection of Majorana Pairs, Phys. Rev. Lett. **118**, 126803 (2017).

[50] G. Burkard and A. Imamoglu, Ultra-long-distance interaction between spin qubits, Phys. Rev. B **74**, 041307(R) (2006).

[51] L. E Bruhat, T. Cubaynes, J. J. Viennot, M. C. Dartiailh, M. M. Desjardins, A. Cottet, and T. Kontos, Strong coupling between an electron in a quantum dot circuit and a photon in a cavity, arXiv:1612.05214 [cond-mat.mes-hall].

[52] M. Leijnse and K. Flensberg, Coupling Spin Qubits via Superconductors, Phys. Rev. Lett. **111**, 060501 (2013).

[53] See Supplemental Material at http://link.aps.org/supplemental/10.1103/PhysRevB.98.155313 for the python code (using the QUTIP package) that calculates the reduced density matrix and the cavity transmission.